

Cold dilute neutron matter on the lattice II: Results in the unitary limit

Dean Lee and Thomas Schäfer

Department of Physics, North Carolina State University, Raleigh, NC 27695

Abstract

This is the second of two papers which investigate cold dilute neutron matter on the lattice using pionless effective field theory. In the unitary limit, where the effective range is zero and scattering length is infinite, simple scaling relations relate thermodynamic functions at different temperatures. When the second virial coefficient is properly tuned, we find that the lattice results obey these scaling relations. We compute the energy per particle, pressure, spin susceptibility, dineutron correlation function, and an upper bound for the superfluid critical temperature.

arXiv:nucl-th/0509018v1 7 Sep 2005

I. INTRODUCTION

This is the second of two papers which investigate cold dilute neutron matter on the lattice using pionless effective field theory. We refer to the first paper as [1]. In this paper we study the scaling behavior of the results in the unitary limit and compute a number of physical observables, the energy and pressure, the spin susceptibility, and the dineutron correlation function.

In the unitary limit the scattering length is much larger than the interparticle spacing whereas the range of the interaction is much smaller. In this limit the only length scales in the problem are $(n_f(\mu))^{-1/3}$ and the thermal wavelength λ_T . Here, $n_f(\mu) = (3\pi^2)^{-1}(2m_N\mu)^{3/2}$ is the density of a free Fermi gas and $\lambda_T = \sqrt{2\pi/(m_NT)}$, where m_N is the neutron mass, μ is the chemical potential, and T is the temperature. All dimensionful quantities can be expressed as suitable powers of either $(n_f(\mu))^{-1/3}$ or λ_T times a function of the dimensionless quantity μ/T . For example, we can write the pressure as [1]

$$P(T, \mu) = \frac{2}{5}\mu n_f(\mu)\mathcal{G}(x) \quad (1)$$

where $x = \mu/T$. Using standard thermodynamic identities one can show that

$$\rho(\mu) = n_f(\mu) \left[\mathcal{G}(x) - \frac{2x}{5}\mathcal{G}'(x) \right], \quad \epsilon = \frac{3P}{2}, \quad (2)$$

where ρ is the density and ϵ is the energy density. In this work we first show how these relations arise in the lattice regularized theory. We then present numerical results for the equation of state, the spin susceptibility, and the dineutron correlation function, and show that the lattice data are consistent with universality.

II. SCALING IN THE UNITARY LIMIT

In this section we derive some scaling relations which relate observables at different temperatures in the unitary limit. Our derivation is equivalent to the treatment in [1]. For the analysis it is simplest to first take the temporal lattice spacing $a_t \rightarrow 0$, and then take the spatial lattice spacing $a \rightarrow 0$. When we take the temporal lattice spacing $a_t \rightarrow 0$, we

end up with a Hamiltonian lattice formulation,

$$\begin{aligned}
H - \mu N &= \sum_{\vec{n}_s, i} \left[\left(-\mu + \frac{3}{m_N} \right) a_i^\dagger(\vec{n}_s) a_i(\vec{n}_s) \right] \\
&\quad - \frac{1}{2m_N} \sum_{\vec{n}, i} \sum_{l_s=1,2,3} \left[a_i^\dagger(\vec{n}_s) a_i(\vec{n} + \hat{l}_s) + a_i^\dagger(\vec{n}_s) a_i(\vec{n}_s - \hat{l}_s) \right] \\
&\quad + C \sum_{\vec{n}_s} a_\uparrow^\dagger(\vec{n}_s) a_\uparrow(\vec{n}_s) a_\downarrow^\dagger(\vec{n}_s) a_\downarrow(\vec{n}_s).
\end{aligned} \tag{3}$$

Here, $a_i(\vec{n}_s)$ is an annihilation operator for a neutron with spin index i at the spatial lattice site \vec{n}_s and C is the coupling constant.

In the unitary limit, which corresponds with $a \rightarrow 0$ and $a_{\text{scatt}} \rightarrow \infty$, it is not difficult to show that

$$C = -\frac{\eta}{m_N}, \tag{4}$$

where η is a constant,

$$\eta = \lim_{L \rightarrow \infty} \frac{L^3}{\sum_{\vec{k} \neq 0} \text{integer} \frac{1}{\Omega_{\vec{k}}}} \simeq 3.957, \tag{5}$$

$$\Omega_{\vec{k}} = 6 - 2 \cos \frac{2\pi k_1}{L} - 2 \cos \frac{2\pi k_2}{L} - 2 \cos \frac{2\pi k_3}{L}. \tag{6}$$

The derivation is as follows. At zero temperature, the value of C can be set by the condition that the two-particle scattering pole occurs at the energy prescribed by Lüscher's formula for energy levels in a periodic box of length L [2, 3]. In the actual lattice simulations we describe later we will determine C in a slightly different way, but the two procedures agree in the limit that the lattice spacing goes to zero. If we place the two-particle scattering pole at energy E_{pole} then the condition on C is

$$-\frac{1}{C} = \lim_{L \rightarrow \infty} \frac{1}{L^3} \sum_{\vec{k} \text{ integer}} \frac{1}{-E_{\text{pole}} + \frac{1}{m_N} \Omega_{\vec{k}}}. \tag{7}$$

Lüscher's formula gives

$$E_{\text{pole}} = \frac{4\pi a_{\text{scatt}}}{m_N L^3} \left[1 + O\left(\frac{a_{\text{scatt}}}{L}\right) \right], \tag{8}$$

We keep a_{scatt} finite for the moment. In the limit $L \rightarrow \infty$ we split the sum in (7) into the term $\vec{k} = 0$ and the remaining terms $\vec{k} \neq 0$,

$$\begin{aligned}
-\frac{1}{C} &= -\frac{1}{L^3} \frac{1}{E_{\text{pole}}} + \frac{1}{L^3} \sum_{\vec{k} \neq 0} \text{integer} \frac{m_N}{\Omega_{\vec{k}}} \\
&= -\frac{m_N}{4\pi a_{\text{scatt}}} + \frac{m_N}{L^3} \sum_{\vec{k} \neq 0} \text{integer} \frac{1}{\Omega_{\vec{k}}}.
\end{aligned} \tag{9}$$

Therefore

$$C = \frac{1}{m_N} \frac{1}{\frac{1}{4\pi a_{\text{scatt}}} - \frac{1}{L^3} \sum_{\vec{k} \neq 0} \text{integer} \frac{1}{\Omega_{\vec{k}}}}. \quad (10)$$

In the unitary limit where $a_{\text{scatt}} \rightarrow \infty$, we have

$$C = -\frac{1}{m_N} \frac{L^3}{\sum_{\vec{k} \neq 0} \text{integer} \frac{1}{\Omega_{\vec{k}}}} = -\frac{\eta}{m_N}, \quad (11)$$

which corresponds with the three-dimensional attractive Hubbard model [4, 5, 6] with

$$\frac{|U|}{t} = 2\eta \simeq 7.914. \quad (12)$$

The grand canonical partition function for our system is

$$Z_G = \text{Tr} \exp [-\beta(H - \mu N)], \quad (13)$$

or

$$Z_G = \text{Tr} \exp \left[\begin{aligned} & \sum_{\vec{n}, i} \left[(\beta\mu - \frac{3\beta}{m_N}) a_i^\dagger(\vec{n}) a_i(\vec{n}) \right] \\ & + \frac{\beta}{2m_N} \sum_{\vec{n}, i} \sum_{l=1,2,3} \left[a_i^\dagger(\vec{n}) a_i(\vec{n} + \hat{l}) + a_i^\dagger(\vec{n}) a_i(\vec{n} - \hat{l}) \right] \\ & + \frac{\beta\eta}{m_N} \sum_{\vec{n}} a_\uparrow^\dagger(\vec{n}) a_\uparrow(\vec{n}) a_\downarrow^\dagger(\vec{n}) a_\downarrow(\vec{n}), \end{aligned} \right] \quad (14)$$

We observe that Z_G is a function of only two parameters, $\frac{\beta}{2m_N}$ and $\beta\mu$. In terms of physical units, these parameters are

$$\frac{\beta}{2m_N} = \frac{1}{2m_N^{\text{phys}} T^{\text{phys}} a^2} = \frac{1}{4\pi} \left(\lambda_T^{\text{phys}} a^{-1} \right)^2, \quad (15)$$

$$\beta\mu = \frac{\mu^{\text{phys}}}{T^{\text{phys}}} = \ln z, \quad (16)$$

where z is the fugacity,

$$z = e^{\beta\mu}. \quad (17)$$

We can take the two independent parameters to be $\lambda_T^{\text{phys}} a^{-1}$ and z .

Consider any operator $F(a_i, a_j^\dagger)$ built from the lattice annihilation and creation operators.

We assume that

$$\langle F \rangle_{\text{continuum}} \equiv \lim_{a \rightarrow 0} \left[a^D \cdot \langle F(a_i, a_j^\dagger) \rangle \right] \quad (18)$$

has a nonzero continuum limit for some power D . We know that

$$\langle F(a_i, a_j^\dagger) \rangle = \frac{\text{Tr} \left[F(a_i, a_j^\dagger) \exp [-\beta(H - \mu N)] \right]}{\text{Tr} [\exp [-\beta(H - \mu N)]]} \quad (19)$$

is a function of only $\lambda_T^{\text{phys}} a^{-1}$ and z . So in order that the factor of a^D drops out of (18), we need in the continuum limit

$$\langle F(a_i, a_j^\dagger) \rangle \rightarrow \left(\lambda_T^{\text{phys}} a^{-1} \right)^D f(z), \quad (20)$$

where $f(z)$ is some function of the fugacity only. Hence

$$\langle F \rangle_{\text{continuum}} = \left(\lambda_T^{\text{phys}} \right)^D f(z) \quad (21)$$

and so

$$\left(\lambda_T^{\text{phys}} \right)^{-D} \langle F \rangle_{\text{continuum}} \quad (22)$$

is a function of z only. We extend this to the case when the operator has an explicit dependence on the displacement, \vec{x}^{phys} . In that case

$$\langle F(\vec{x}^{\text{phys}}) \rangle_{\text{continuum}} \equiv \lim_{a \rightarrow 0} \left[a^D \cdot \langle F(a_i, a_j^\dagger, \vec{x}^{\text{phys}} a^{-1}) \rangle \right], \quad (23)$$

where $\vec{x}^{\text{phys}} a^{-1}$ is the displacement in lattice units. Therefore

$$\left(\lambda_T^{\text{phys}} \right)^{-D} \langle F(\vec{x}^{\text{phys}}) \rangle_{\text{continuum}} = f \left(z, \vec{x}^{\text{phys}} (\lambda_T^{\text{phys}})^{-1} \right). \quad (24)$$

As an example we show that the particle density times three powers of the thermal wavelength is a function of only the fugacity. The particle density in the continuum limit is

$$\langle \rho \rangle_{\text{continuum}} = \lim_{a \rightarrow 0} \left[a^{-3} \cdot \langle a_\uparrow^\dagger(\vec{n}_s) a_\uparrow(\vec{n}_s) + a_\downarrow^\dagger(\vec{n}_s) a_\downarrow(\vec{n}_s) \rangle \right], \quad (25)$$

where the expectation value can be measured at any spatial lattice site \vec{n}_s . Therefore $D = -3$ and

$$\left(\lambda_T^{\text{phys}} \right)^3 \langle \rho \rangle_{\text{continuum}} \quad (26)$$

is a function of only the fugacity. Similarly the energy per particle times inverse temperature,

$$\beta \frac{E}{A}; \quad (27)$$

pressure times inverse temperature and three powers of the thermal wavelength,

$$\left(\lambda_T^{\text{phys}} \right)^3 \beta P; \quad (28)$$

and Fermi energy times inverse temperature,

$$\beta E_F = \beta \frac{(3\pi^2 \rho)^{2/3}}{2m_N}; \quad (29)$$

are all functions of fugacity only.

Using the unitary limit scaling relations we can derive a simple relation between the energy density and pressure [1]. The energy density is

$$\begin{aligned} \frac{E}{V} &= -\frac{1}{V} \frac{\partial}{\partial \beta} \ln Z_G + \mu \rho \\ &= -\frac{1}{V} \left[\frac{\partial}{\partial \beta} - \frac{\mu}{\beta} \frac{\partial}{\partial \mu} \right] \ln Z_G. \end{aligned} \quad (30)$$

We note that

$$\left(\lambda_T^{\text{phys}} \right)^3 \frac{1}{V} \ln Z_G = \left(\lambda_T^{\text{phys}} \right)^3 \beta P, \quad (31)$$

which is only a function of fugacity. Since

$$\left[\frac{\partial}{\partial \beta} - \frac{\mu}{\beta} \frac{\partial}{\partial \mu} \right] z = \left[\frac{\partial}{\partial \beta} - \frac{\mu}{\beta} \frac{\partial}{\partial \mu} \right] e^{\beta \mu} = 0, \quad (32)$$

we have the result

$$\begin{aligned} \frac{E}{V} &= -\frac{1}{V} \left[\frac{\partial}{\partial \beta} - \frac{\mu}{\beta} \frac{\partial}{\partial \mu} \right] \ln Z_G \\ &= -\frac{1}{V} \left(\lambda_T^{\text{phys}} \right)^3 \frac{1}{V} \ln Z_G \left[\frac{\partial}{\partial \beta} - \frac{\mu}{\beta} \frac{\partial}{\partial \mu} \right] \left[\left(\lambda_T^{\text{phys}} \right)^{-3} \right] \\ &= \frac{3}{2\beta} \frac{1}{V} \ln Z_G = \frac{3}{2} P. \end{aligned} \quad (33)$$

III. RESULTS

In the following we present lattice simulation results for cold dilute neutron matter in the unitary limit. We use a spatial lattice spacing of $a = (50 \text{ MeV})^{-1}$ and temporal lattice spacing of $a_t = (24 \text{ MeV})^{-1}$. The temporal lattice spacing is sufficiently small that the results are close to the $a_t \rightarrow 0$ limit. We use the hybrid Monte Carlo algorithm [7] to generate Hubbard-Stratonovich field configurations as described in [8]. We use diagonal preconditioning before each conjugate gradient solve as described in [I].

The finite volume error was tested by going to larger volumes, and the final lattice sizes were chosen so that the finite volume error was less than one percent. The lattice dimensions

we used for the various temperatures are shown in Table 1.

Table 1: Lattice volumes for various temperatures

T (MeV)	L	L_t
4	4	6
3	5	8
2	5	12
1.5	6	16
1	6	24

We adjust the coefficient C of the four-fermion interaction as suggested in [I]. For each temperature and lattice volume, we compute the density for both free lattice fermions and for lattice regularized two-particle bubbles. We use the free fermion result in order to determine the first virial coefficient $b_1(T)$ (see Table 1 in [I]) and the bubble sum to compute the second virial coefficient $b_2(T)$,

$$\rho^{\text{bubble}} \approx \frac{2}{\lambda_T^3} b_1(T) [z + 2 \cdot b_2(T) z^2]. \quad (34)$$

We then adjust C so that

$$b_2(T) = 3 \cdot 2^{-\frac{5}{2}}. \quad (35)$$

This constraint is also used to compute the derivative of C with respect to the temporal lattice spacing. The results for $C(T)$ and $\frac{dC}{d\alpha_t}$ are shown in Table 2.

Table 2: C and $\frac{dC}{d\alpha_t}$ on the lattice

T (MeV)	C (10^{-4} MeV $^{-2}$)	$\frac{dC}{d\alpha_t}$ (10^{-5} MeV $^{-2}$)
4	-0.971	-0.76
3	-0.948	-1.40
2	-0.958	-2.12
1.5	-0.987	-2.47
1	-1.043	-2.68
0.667	-1.098	-2.65
0.5	-1.128	-2.52

For each temperature we have probed densities up to a quarter-filled lattice. With a spatial lattice spacing of $(50 \text{ MeV})^{-1}$, the quarter-filled lattice corresponds with a density of 0.0081 fm^{-3} . Beyond this one might find significant lattice artifacts.

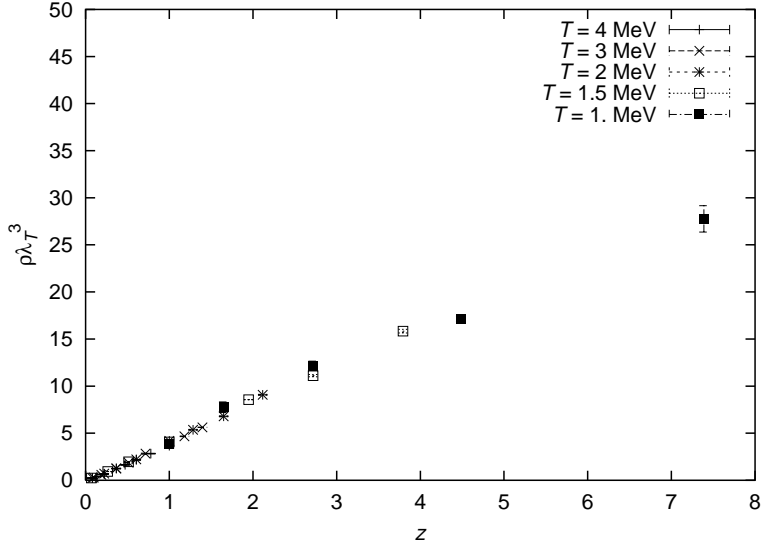


FIG. 1: Density times λ_T^3 versus fugacity for various temperatures.

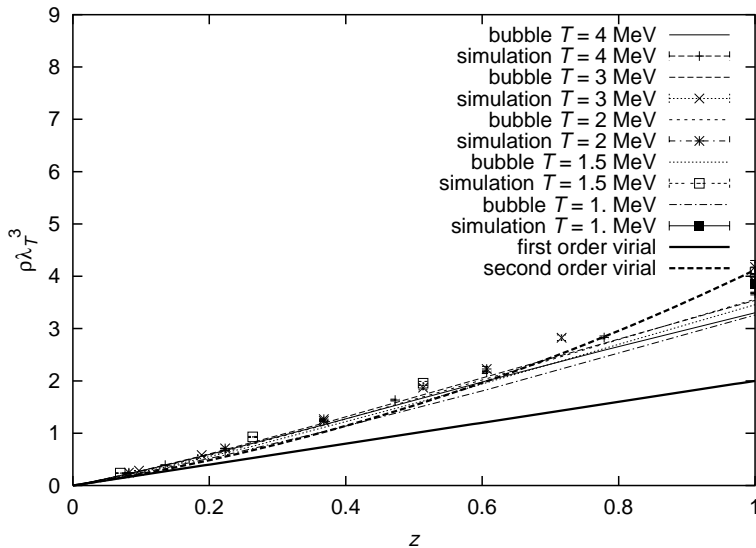


FIG. 2: Density times λ_T^3 versus fugacity for small fugacity. We also include comparisons with the virial expansion at first and second orders.

A. Density versus fugacity

In Fig. 1 we plot the density times λ_T^3 versus fugacity for temperatures $T = 4, 3, 2, 1.5,$ and 1 MeV. The data from the five different temperatures appear to fall on a single curve. This suggests that $\rho\lambda_T^3$ depends only on z , as predicted by unitary limit scaling. In Fig. 2 we magnify the plot of $\rho\lambda_T^3$ at low fugacity, showing both bubble chain results and full simulation results. We show the first order and second order virial results with

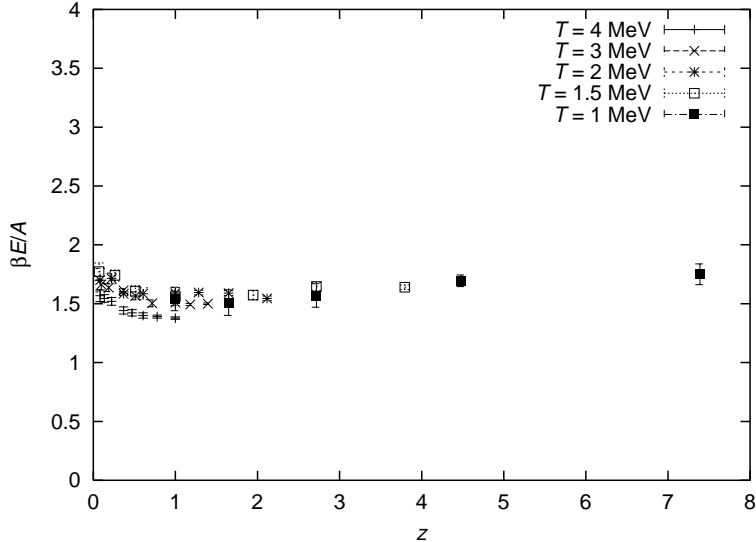


FIG. 3: Energy per particle times β versus fugacity. We show results for $T = 4, 3, 2, 1.5,$ and 1 MeV.

$$b_2(T) = 3 \cdot 2^{-\frac{5}{2}} \approx 0.530. \quad (36)$$

Since we have tuned the interaction coefficient to produce the correct second order virial coefficient, it is not surprising that the lattice data agrees with the virial expansion at low fugacity.

B. Energy per particle versus fugacity

In Fig. 3 we plot the energy per particle times β versus fugacity for temperatures $T = 4, 3, 2, 1.5,$ and 1 MeV. The energy per particle times β appears to depend only on fugacity, as predicted by scaling in the unitary limit. The small deviation for different temperatures appears to be due mainly to an overall shift in the height of the curves. In the continuum limit at $z = 0$, we expect the equipartition result

$$\frac{\beta E}{A} = \frac{3}{2}. \quad (37)$$

The slight deviations from $\frac{3}{2}$ at $z = 0$ can be attributed to lattice cutoff effects in the free particle kinetic energy.

In Fig. 4 we magnify the same plot for small fugacity and include both bubble chain calculation results and full simulation results. We also show the first and second order virial

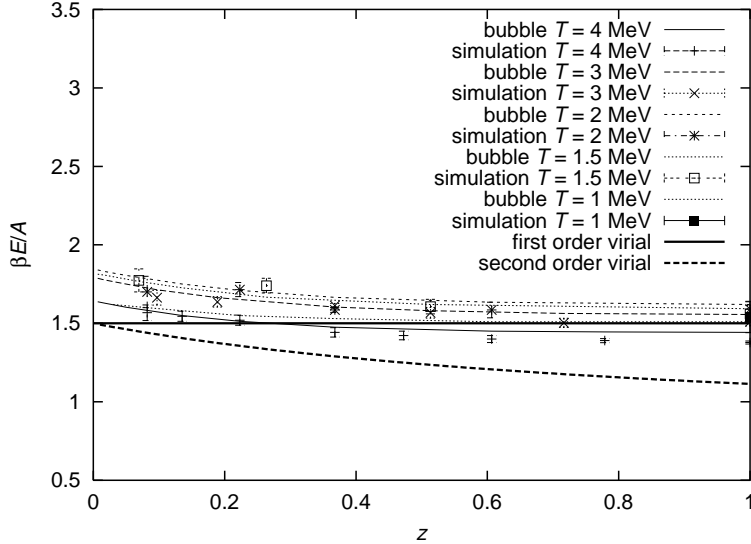


FIG. 4: Energy per particle times β versus fugacity at small fugacity. We compare with first and second order virial expansion results.

results in the continuum. At first order we have

$$\frac{\beta E}{A} = \frac{3}{2}, \quad (38)$$

and at second order,

$$\frac{\beta E}{A} = \frac{\left(\frac{3}{2} - \ln z\right) z + \frac{3}{4\sqrt{2}} \left(\frac{3}{2} - 2 \ln z\right) z^2}{z + \frac{3}{2\sqrt{2}} z^2} + \ln z. \quad (39)$$

We see that apart from small shifts in the overall height, the lattice results agree with the continuum virial results.

C. Energy density and pressure

In Fig. 5 we show the energy density times $\beta\lambda_T^3$ versus fugacity for temperatures $T = 4, 3, 2, 1.5,$ and 1 MeV. Scaling in the unitary limit requires that the energy density times $\beta\lambda_T^3$ is only a function of fugacity, and this appears to be the case. In Fig. 5 we also plot the pressure times $\frac{3}{2}\beta\lambda_T^3$, which according to (33) should equal the energy density times $\beta\lambda_T^3$. We have computed the pressure by numerical integration of the density as a function of chemical potential,

$$P = \frac{T}{V} \ln Z_G = \frac{1}{V} \int_{-\infty}^{\mu} A(\mu') d\mu' = \int_{-\infty}^{\mu} \rho(\mu') d\mu'. \quad (40)$$

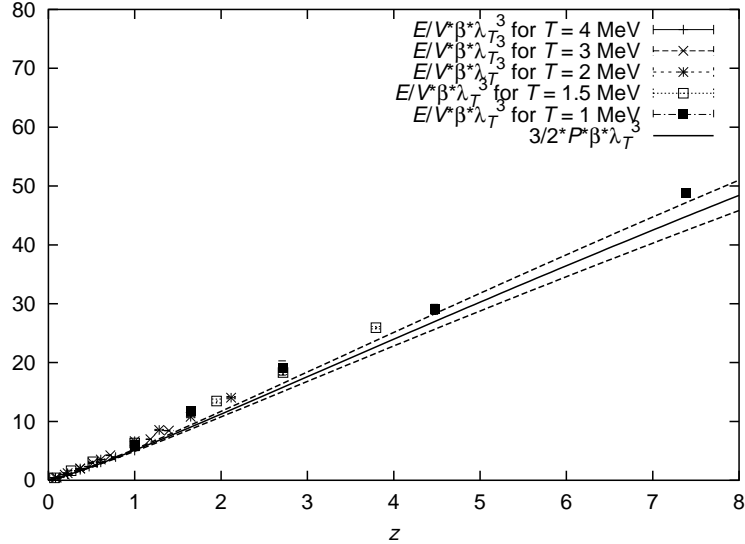


FIG. 5: Energy density times $\beta\lambda_T^3$ versus fugacity for various temperatures. We compare with the pressure times $\frac{3}{2}\beta\lambda_T^3$.

We see that the lattice results appear to confirm the unitary limit relation,

$$\frac{E}{V} = \frac{3}{2}P. \quad (41)$$

D. Reduced energy versus reduced temperature

In units where Boltzmann's constant equals 1, the degeneracy temperature T_F is the same as the Fermi energy,

$$T_F = E_F = \frac{(3\pi^2\rho)^{2/3}}{2m_N}. \quad (42)$$

In Fig. 6 we plot the energy per particle divided by $\frac{3}{5}E_F$ versus the temperature divided by T_F for temperatures $T = 4, 3, 2, 1.5,$ and 1 MeV. As expected from unitary limit scaling all points appear to lie on a single curve. In Fig. 7 we show a magnified plot of the energy per particle divided by $\frac{3}{5}E_F$ versus the temperature divided by T_F . The data points at the lowest values of T/T_F appear to lie on straight line with intercept

$$\frac{E/A}{\frac{3}{5}E_F} = 0.07. \quad (43)$$

One expects the curve to reach $T/T_F = 0$ with zero slope. The actual intercept at $T/T_F = 0$, which corresponds with the parameter ξ in the zero temperature relation,

$$\frac{E}{A} = \xi \frac{3}{5} \frac{k_F^2}{2m}, \quad (44)$$

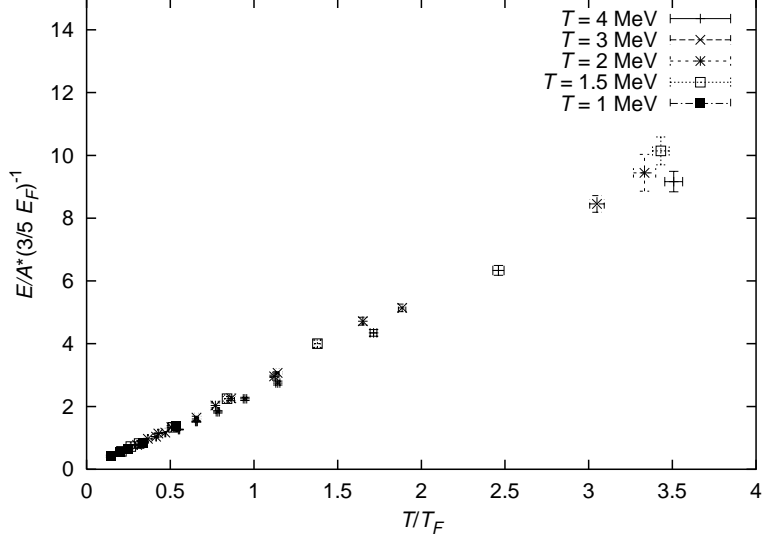


FIG. 6: The energy per particle divided by $\frac{3}{5}E_F$ versus temperature divided by T_F for temperatures $T = 4, 3, 2, 1.5,$ and 1 MeV.

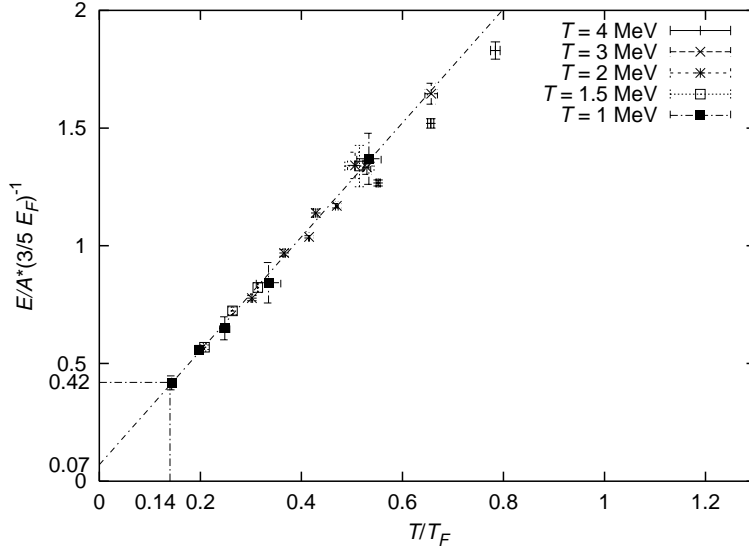


FIG. 7: A magnified plot at low temperatures of the energy per particle divided by $\frac{3}{5}E_F$ versus temperature divided by T_F .

should likely be somewhere between 0.07 and 0.42. Since there is no noticeable nonanalytic behavior in the data shown, this suggests that the superfluid critical temperature T_C should satisfy

$$\frac{T_C}{T_F} < 0.14. \quad (45)$$

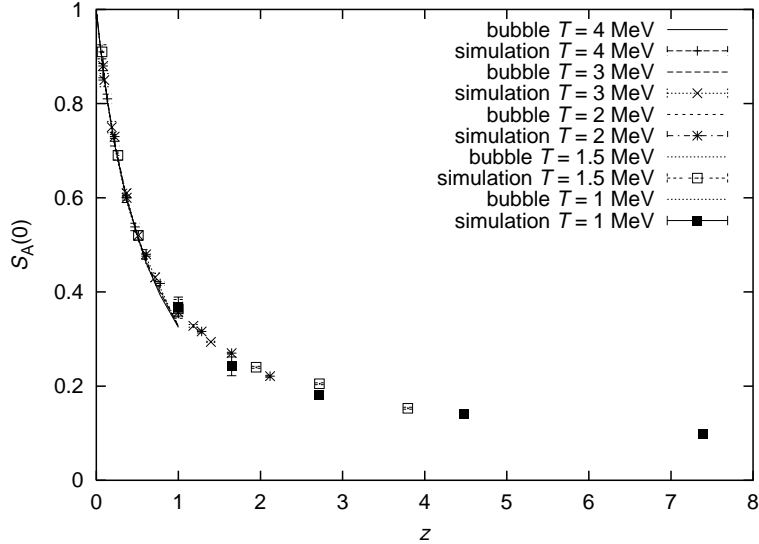


FIG. 8: Lattice results for the axial response as a function of fugacity for temperatures $T = 4, 3, 2, 1.5,$ and 1 MeV.

E. Axial response and spin susceptibility

The axial response at zero momentum is defined as [9]

$$S_A(0) = \frac{1}{\langle N \rangle} \langle (N_\uparrow - N_\downarrow)(N_\uparrow - N_\downarrow) \rangle, \quad (46)$$

where $N_{\uparrow(\downarrow)}$ is the number operator for spin up(down) neutrons. N is the total number operator so that

$$\langle N \rangle = \langle N_\uparrow + N_\downarrow \rangle = A. \quad (47)$$

$S_A(0)$ is a dimensionless quantity with a finite continuum limit and therefore should be a function of fugacity only. It is normalized to equal 1 at zero density. $S_A(0)$ is proportional to the Pauli spin susceptibility [5, 6],

$$\chi_P = \frac{1}{\langle N \rangle T} \sum_{\vec{n}_s, \vec{n}'_s} \left\langle \left[a_i^\dagger(\vec{n}_s) [\vec{\sigma}]_{ij} a_j(\vec{n}_s) \right] \cdot \left[a_k^\dagger(\vec{n}'_s) [\vec{\sigma}]_{kl} a_l(\vec{n}'_s) \right] \right\rangle = \frac{3S_A(0)}{T}. \quad (48)$$

In Fig. 8 we show the axial response as a function of fugacity for temperatures $T = 4, 3, 2, 1.5,$ and 1 MeV. The lattice results for the axial response appear to lie on one curve, as predicted by the unitary limit scaling relations.

The decrease in the axial response indicates that the transfer of spin from one spatial region to another is being suppressed. This is due to the formation of spin zero pairs. A

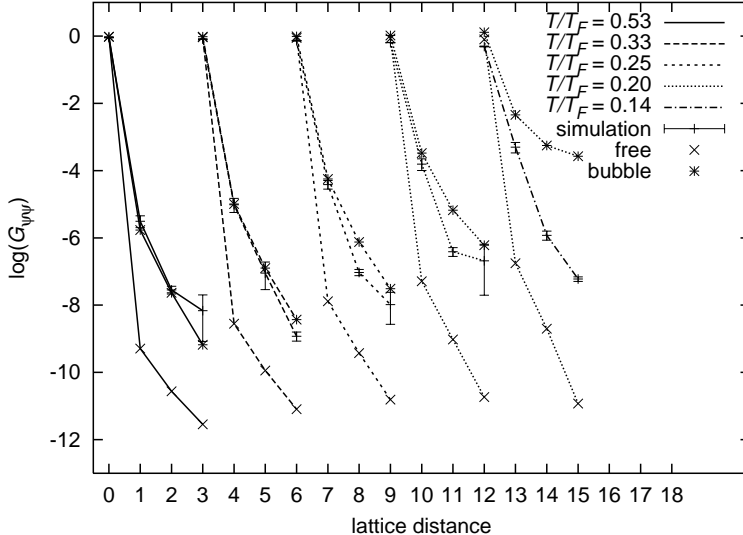


FIG. 9: Logarithm of the dineutron correlation function versus lattice distance measured along a lattice axis. We show results for $T = 1$ MeV.

superfluid transition leads to nonanalytic behavior in the susceptibility. A sharp crossover in the susceptibility can be used to define a pseudogap phase. We do not observe any of these phenomena. The susceptibility becomes quite small for the most degenerate systems studied, but the dependence on temperature is smooth.

F. Dineutron correlation function

We define the equal-time dineutron correlation function as

$$G_{\psi\psi}(\vec{n}_s) = \left\langle a_{\downarrow}(\vec{n}_s) a_{\uparrow}(\vec{n}_s) a_{\uparrow}^{\dagger}(0) a_{\downarrow}^{\dagger}(0) \right\rangle. \quad (49)$$

In Fig. 9 we show the logarithm of the dineutron correlation function as a function of lattice distance measured along a lattice axis. We show results for $T = 1$ MeV and various values of T/T_F . We have staggered the plots for better viewing, and the five highest points represent data measured at zero lattice distance. For comparison we also show the free dineutron correlation function as well as the result of the bubble chain approximation. We observe that the interacting correlation function is larger than the non-interacting one for all temperatures. This reflects the attractive interaction in the spin zero channel. At the higher temperatures the correlation function is quantitatively explained by the bubble chain approximation. At $T/T_F = 0.14$ the bubble chain correlator starts to level off, indicative of

long range order, but the full correlation function does not. This implies that $T_C/T_F < 0.14$.

IV. SUMMARY

We have studied neutron matter in the unitary limit on the lattice. In [I] we concentrated on the low density/high temperature equation of state and compared the results to the virial expansion. We found significant finite lattice spacing errors and suggested that the scaling behavior can be improved by tuning the second virial coefficient rather than the zero temperature scattering length.

In part II we showed that tuning the second virial coefficient improves universal scaling for the entire range of densities and temperatures studied. We found, in particular, that the energy per particle in units of T_F only depends on μ/T and that the energy density is 3/2 times the pressure. In the temperature range studied the energy per particle in units of T_F is essentially linear in T/T_F . This means that at present we can only provide bounds on the universal parameter ξ . We find $0.07 \leq \xi \leq 0.42$. This result is marginally consistent with the Green function Monte Carlo result $\xi = 0.44$ [10].

We also studied the spin susceptibility and the dineutron correlation function. We find that the spin susceptibility is strongly suppressed in the most degenerate systems, but no clear phase transition is observed. We also find that the dineutron correlation function is strongly enhanced over the free correlation function, but no long range order is observed. We conclude that the critical temperature for the the transition to a superfluid phase is less than $0.14T_F$. This bound is lower than the result $T_C = 0.22(3)T_F$ [11] but consistent with the result $T_C = 0.035(4)T_F$ obtained in [12]. Green's function Monte Carlo calculations are restricted to $T = 0$ and can only determine the gap, not the critical temperature. Carlson, et. al., [10] find $\Delta = 0.9 \cdot \frac{3}{5}E_F$. If the critical temperature were related to the gap by $T_C = 0.57\Delta$ as in BCS theory this would imply $T_C = 0.31T_F$, but there is no reason to expect this relation to hold in the unitary limit.

Acknowledgments: This work is supported in part by the US Department of Energy grants DE-FG-88ER40388 (T.S.) and DE-FG02-04ER41335 (D.L.).

[1] T.-L. Ho, Phys. Rev. Lett. **92**, 090402 (2004).

- [2] M. Lüscher, Commun. Math. Phys. **105**, 153 (1986).
- [3] S. R. Beane, P. F. Bedaque, A. Parreno, and M. J. Savage, Phys. Lett. **B585**, 106 (2004), hep-lat/0312004.
- [4] J. Hubbard, Proc. Roy. Soc. **276**, 238 (1963).
- [5] A. Sewer, X. Zotos, and H. Beck, Phys. Rev. B **66**, 140504(R) (2002), cond-mat/0204053.
- [6] R. dos Santos, Phys. Rev. B **50**, 635 (1994).
- [7] S. Duane, A. D. Kennedy, B. J. Pendleton, and D. Roweth, Phys. Lett. **B195**, 216 (1987).
- [8] D. Lee and T. Schaefer, Phys. Rev. **C72**, 024006 (2005), nucl-th/0412002.
- [9] A. Burrows and R. F. Sawyer, Phys. Rev. **C58**, 554 (1998), astro-ph/9801082.
- [10] J. Carlson, S. Y. Chang, V. R. Pandharipande, and K. Schmidt, Phys. Rev. Lett. **91**, 50401 (2003), physics/0303094.
- [11] A. Bulgac, J. E. Drut, and P. Magierski (2005), cond-mat/0505374.
- [12] M. Wingate (2005), cond-mat/0502372.

